



Investigation about the cause of the intense pre-monsoon cyclonic system over the Bay of Bengal

Pankaj Lal Sahu¹ · Sandeep Pattnaik¹

Received: 8 February 2024 / Accepted: 17 August 2024

© The Author(s), under exclusive licence to Springer-Verlag GmbH Austria, part of Springer Nature 2024

Abstract

A 41-year dataset from 1982 to 2022 analyzed climatic patterns influencing cyclone formation in the Bay of Bengal (BoB). Results showed a significant increase in sea surface temperature (SST) and a warming trend over the past four decades. Specific humidity increased while wind shear decreased. The moisture budget showed increased precipitation and evaporation rates, possibly due to more warming scenarios. Tropical Cyclones (TC) experienced significant increases in SST anomalies. These anomalies were higher during cyclonic than non-cyclonic years, except for 2015, due to El Niño conditions. Tropical Cyclone Heat Potential (TCHP) values increased in cyclonic years, while specific humidity (SH) anomalies increased 10–15 days before cyclone formation. Moist static energy (MSE) values increased across the BoB region, with TCs Amphan, Yaas, and Asani exhibiting significant positive relative vorticity (RV) anomalies. The Madden-Julian Oscillation (MJO) plays a crucial role in TC initiation and intensification, with recent TC demonstrating this. In general, the Empirical Orthogonal Function (EOF) analysis of SST, upper-level moisture, and low wind shear for May over the BoB reveals more conducive conditions for TC intensification. Furthermore, it is also found that the negative phase of the Indian Ocean Dipole (NIOD) associated pre-monsoon month of May has produced more intense TCs in recent years over BoB. The findings of this study will facilitate augmenting existing knowledge and understanding about the genesis and intensification of pre-monsoon TCs over BoB.

1 Introduction

Tropical cyclones (TCs) are devastating in nature and have direct effects such as strong winds, heavy rain, storm surges, and loss of lives, as well as indirect effects such as damage to coral reefs, spread of disease, and economic disruption. Low wind shear, warm sea surface temperature, ocean heat content, and high specific humidity are major conducive parameters for TC formation, creating a cyclonic vortex that can span hundreds of miles in diameter (Rai et al. 2016; Chakraborty et al. 2022). Furthermore, the genesis and progression of tropical cyclones can be subject to the effects of various other factors, including the spatial positioning of the Intertropical Convergence Zone (ITCZ), the existence

of upper-level outflow, and the amount of moisture in the atmosphere. (Berry and Reeder 2014; Vishwakarma and Pattnaik 2022).

In the 21st century, extreme weather events, including tropical cyclones, have become more frequent and severe worldwide due to climate change. As projected global temperatures rise by 2 °C due to human activities, we expect significant impacts on tropical cyclone (TC) activity. This analysis reveals a strong link between rising sea levels and increased storm flooding. Global TC precipitation rates will likely rise by approximately 14%, and lifetime maximum surface wind speeds are projected to increase by a median of 5%. This suggests that TCs will become more intense in the future. Projections also indicate a 13% increase in the global proportion of TCs reaching highly intense levels, specifically category 4 to 5 storms (Knutson et al. 2020; Balaguru et al. 2016).

The Bay of Bengal (BoB) basin is the most active and significant tropical cyclone-prone region and is susceptible to the formation of tropical cyclones. It has two primary cyclone seasons: pre-monsoon (April to June) and post-monsoon (October to December). Recently, every year in the

Communicated by Clemens Simmer, Ph.D.

✉ Sandeep Pattnaik
spt@iitbbs.ac.in

¹ School of Earth, Ocean and Climate Sciences, Indian Institute of Technology Bhubaneswar, Argul, Jatni, Khurda, Odisha 752050, India

pre-monsoon month (particularly May), ferocious cyclones are brewing and making landfall, causing catastrophic deaths and devastation in the region (i.e., India, Bangladesh, Myanmar, and Sri Lanka). The basin witnesses a wide range of cyclone intensities, from relatively weak tropical storms to extremely powerful cyclonic storms (super cyclone) (Priya et al. 2022; Mondal et al. 2022). This cyclone basin has a long history of the deadliest TCs on record, such as the 1970 Bhola Cyclone, the 1991 Bangladesh Cyclone, and the 1999 Odisha Cyclone, which occurred in this basin, resulting in catastrophic loss of life and property (Hossain 2017; Chowdhury et al. 1993; Fanchiotti et al. 2020). Storm surges, heavy rainfall, and flooding are common, causing significant humanitarian and economic crises (Mishra and Malakar 2020).

Pre-monsoon tropical cyclones are a significant hazard to the coastal communities of the BoB. These cyclones typically form in April and May, before the onset of the monsoon season. The BOB is a semi-enclosed basin, which means that it is surrounded by land on three sides. This can trap cyclones and prevent them from moving away from the coast (WMO Technical Document 2008). The BoB is also home to a large population, which makes it more vulnerable to the impacts of cyclones. The most intense pre-monsoon cyclone in the last 10 years was Cyclone Amphan, which made landfall in West Bengal and Bangladesh in May 2020. Amphan was a Category 5 equivalent cyclone with sustained winds of 240 km/h. In the last 4–5 years, every year, intensified cyclones (> 89 km/h) have been formed over BoB in the pre-monsoon season (Vishwakarma et al. 2022). Recent advancements have improved the accuracy of TC track predictions. However, accurately forecasting TC intensity and direction still poses challenges (Wang et al. 2022). Enhancing predictive precision is crucial for regional disaster management, enabling proactive mitigation strategies. Extensive research combining observations and simulations has shed light on TC characteristics. Yet, a comprehensive understanding of TC behavior remains incomplete, leading to uncertainties in longer-term predictions.

This research paper aims to examine the changes in local and large-scale meteorological conditions during recent pre-monsoon years that have contributed to the development of consecutive intensified cyclonic events over BoB. The data used and the methodology implemented are outlined in Sect. 2. Subsequently, the results are meticulously presented in Sect. 3. Finally, a concise summary of the results is provided in Sect. 4.

2 Data and methodology

Various data sets were utilized to investigate atmospheric conditions over 41 years (1982–2022). These data sets included upper-level specific humidity (200–500 hPa), lower-level specific humidity (600–1000 hPa), meridional and zonal components of wind (200 and 850 hPa), precipitation rate, evaporation rate, total column water vapour, vertically integrated moisture divergence, and geopotential. The data was obtained from ERA5, a widely used atmospheric reanalysis dataset, at a horizontal resolution of $0.25^\circ \times 0.25^\circ$ (Hersbach et al. 2023). The study aimed to assess long-term trends in these atmospheric variables and also examine the conditions 15 days before the development of cyclonic storms.

To examine the ocean surface conditions in the Bay of Bengal, we use daily sea surface temperature (SST) data obtained from the Optimum Interpolation Sea Surface Temperature (OISST) at 0.25° horizontal resolution (Huang et al. 2021). Monthly ocean heat content from the surface down to 300 m depth (OHC300) at 0.25° horizontal resolution is taken from Ocean Reanalysis System 5 (ORAS5) (available from <https://cds.climate.copernicus.eu/cdsapp#!/dataset/reanalysis-oras5>). Tropical Cyclone Heat Potential (TCHP) daily data from 1993 to 2022 is collected from the Bhuvan portal (available from <https://bhuvan-app3.nrsc.gov.in/data/download/index.php>).

This study aims to assess the significance of the various components of the moisture conservation equation; the atmospheric moisture budget can be expressed as (Banacos et al. 2005).

$$P - E = -dPW + MFC \quad (1)$$

$$MFC = -\nabla \cdot (qV_h) = -V_h \cdot \nabla q - q \nabla \cdot V_h \quad (2)$$

$$MFC = \underbrace{-u \partial q / \partial x - v \partial q / \partial y}_{\text{Advection term}} - \underbrace{q (\partial u / \partial x + \partial v / \partial y)}_{\text{Convergence term}} \quad (3)$$

where the variables P , E , MFC , PW , q , V_h , u , and v represent precipitation, surface evaporation, the convergence of vertically integrated horizontal water vapour flux, total column water vapour or precipitable water, specific humidity, horizontal velocity vector, zonal velocity, and meridional velocity, respectively.

Moist static energy (MSE) is the sum of internal energy, potential energy, and latent energy (Neelin and Held 1987; Back and Bretherton 2006).

$$MSE = c_p T + gz + l_v q \quad (4)$$

where dry air's specific heat capacity at constant pressure is $c_p = 1.005 \text{ kJ kg}^{-1} \text{ K}^{-1}$, where T is temperature, $g = 9.8 \text{ ms}^{-2}$ is gravity acceleration, z is height, $L_v = 2256 \text{ kJ kg}^{-1}$ is the latent heat of condensation. MSE is computed by taking the average over the vertical column (1000–200 hPa levels).

Data from the Australian Bureau of Meteorology (<http://www.bom.gov.au/climate/mjo/>) is utilized to assess the Madden-Julian Oscillation's (MJO) phase and amplitude impact on cyclone formation. The Real-time Multivariate (RMM) index employs the first two empirical orthogonal functions (EOFs), RMM1 and RMM2, over the 15°S–15°N region for OLR, 850 hPa, and 200 hPa wind data (Wheeler and Hendon, 2004). Empirical Orthogonal Functions (EOF) analysis decomposes geophysical field variations, identifying orthogonal spatial patterns combined with their principal components (PC) linearly (Lorenz 1956). The analysis spans May from 1982 to 2022 and examines sea surface temperature (SST), wind shear, and specific humidity. Positive and negative Indian Ocean Dipole (IOD) events are obtained from the Japan Meteorological Agency (<https://ds.data.jma.go.jp/tcc/tcc/products/elnino/iodevents.html>).

For this study, recent 4 land falling cyclones (severe cyclonic storm or above category) over BoB are selected from the last decade (i.e. 2011–2022). These are Fani (2019), Amphan (2020), Yaas (2021), and Asani (2022). In addition, three cases of non-cyclonic pre-monsoon years 2011, 2012, and 2015 over the BoB are also considered for comparison purpose within the same decade. The objective of this investigation is to gain a comprehensive understanding of the underlying phenomena associated with the formation of these recent intense pre-monsoon cyclones. The duration of the study spanned over 15 days preceding the onset of the cyclonic storm (CS) phase, and for non-cyclonic years, it is nearly common 15 days coherent with the cyclonic years dates in May (i.e., 8 to 22 May).

3 Results and discussion

3.1 Long-term trends

To perform a thorough analysis of the persistent climatic patterns influencing the formation of cyclones in the BoB in May, we undertook a detailed investigation of a time series dataset spanning 41 years, from 1982 to 2022. The scope of our analysis includes various essential meteorological variables, each of which plays a pivotal role in shaping the behavior and intensity of cyclones in this region. Primarily, examination of SST patterns demonstrates a prominent increasing trend (Fig. 1a). It indicates a steady pattern until 2004, after which subsequent findings reveal a significant and enduring trend of warming during the most recent

decades. Over the past four decades, there has been a notable increase in SST, amounting to approximately 0.5 °C. Concurrently with SST, OHC trends closely mirror those of SST, demonstrating an enduring pattern of increase over the study period. Noteworthy observations include the lowest OHC recorded in 2018 and the highest in 2016, aligning seamlessly with the SST trends observed in the past decade.

The specific humidity at both the upper and lower levels is shown in Fig. 1b. There has been a noticeable upward trend in both upper and lower-level SH, but the lower level exhibits a rather modest rise. In recent decades, both lower and upper SH have seen a similar trend. Figure 1c illustrates the wind shear, wherein a noticeable decrease in wind shear of around 1 m/s is noted during four decades. Also illustrated in Fig. 1d is a marginal upward trend in upper-level wind divergence and lower-level relative vorticity particularly in the last decade. The analysis done shows a clear indication of favourable conditions for the formation of tropical cyclones. However, it is crucial to recognize the significant annual fluctuations observed in these climatic factors. These fluctuations underscore the dynamic nature of the Bay of Bengal's climatic system. To better understand the factors contributing to the recent occurrence of intense cyclones, a more detailed analysis of daily conditions is necessary.

To further understand the moisture budget over the past decades, an analysis has been done on different terms of the budget equation. Figure 2a shows the precipitation and evaporation rate; it shows that both precipitation and evaporation have increased during the decades. The precipitation rate increased by 1 mm/day, while the evaporation rate increased by 0.5 mm/day. Figure 2b shows the dPW and moisture flux divergence. It shows that the dPW term is very small and hasn't changed over the years, but there has been a slight increase in moisture convergence. The whole moisture budget suggests that increasing evaporation rate has contributed to more precipitation, while there has also been an observed rise in moisture convergence. The increase in evaporation rate may be due to more warming scenarios.

3.2 Conditioning before TC formation

Figure 3a, b, c, d shows SST anomalies 15 days prior to the formation of the CS phase of Fani (2019), Amphan (2020), Yaas (2021), and Asani (2022), respectively. It is clear that the SST was 1 to 1.2 °C higher, majorly in 5 to 10°N as CS started to form near 5°N. In the case of Amphan and Yaas, the SST anomaly reached 2°C, and in the case of Asani, it reached a maximum of 1.9 °C. All these years have higher SST anomaly when compared to non-stormy years 2011, 2012, and 2015 (Fig. 3e, f,g), where these anomalies were negative except for the case of 2015, where SST anomaly reached up to 1.2 °C. 2015 has been seen as an exception

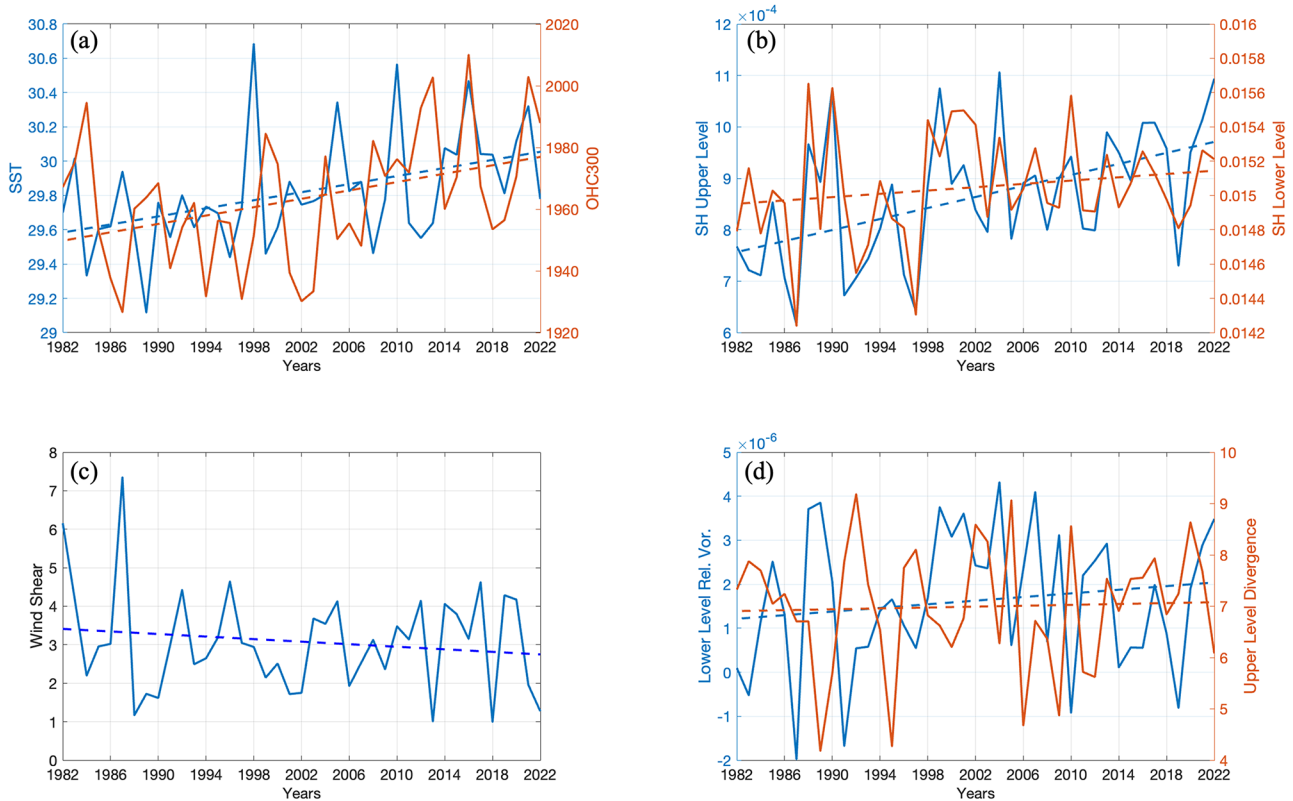


Fig. 1 Time series of (a) SST (°C) on the left axis and on the right axis OHC300 (kJ/cm²), (b) SH (kg/kg) for upper level (200–500 hPa) on the left axis and for lower level (600–1000 hPa) on the right axis, (c) Wind shear (m/s), (d) Lower level (600–900 hPa) relative vorticity

(s⁻¹) on the left axis and upper level (200–500 hPa) divergence (s⁻¹) on the right axis. The dashed line shows the trend line of the respective parameters

case as SST is been higher because 2015–16 was the strongest El Niño years in the last three decades (Iskandar et al. 2018). TCHP represents the amount of heat stored in the upper ocean layers (up to 26 °C isotherm) that can potentially be transferred to the atmosphere. This heat serves as the primary energy source for tropical cyclones. As the storm moves over warm ocean waters with high TCHP, it can extract heat energy from the ocean, which fuels the cyclone's convective processes and strengthens the storm. It plays an important role in TC development and intensification (Wada and Usui 2007). TCHP in Fig. 4 shows the same signatures as SST with a 70–100 kJ/cm² increase in TCHP values before CS formation and these values are mostly negative in non-stormy years with the exception of year 2015.

Specific humidity, a measure of the absolute amount of water vapour present in the air, plays a crucial role in the formation, intensification, and behaviour of tropical cyclones. Specific humidity is directly related to the amount of latent heat energy available in the atmosphere. As warm, moist air rises from the ocean's surface, it cools and releases latent heat as water vapour condenses into liquid water. This released heat provides the primary source of energy

for tropical cyclones, driving their convective processes and intensification. Higher specific humidity means more moisture available for condensation, leading to stronger and more powerful storms. TC requires a constant supply of warm, moist air to sustain itself. Areas with high specific humidity provide a steady source of moisture that can be drawn into the storm's circulation.

Figures 5 and 6 show the specific humidity anomaly hovmoller (averaged over 5–25 N) at upper and lower levels, respectively. In the case of Fani, from 10 days before the development of the CS phase, SH started to increase; during Amphan, it started increasing similarly 10 days prior, covering the whole BoB nearly 5 days before. In the case of Yaas, the increase was nearly 5 days before negative anomalies were seen, and in Asani, it was nearly 7 days. The rise in all the Stormy years is about $0.4 \times 10^{-3} - 0.45 \times 10^{-3}$ kg/kg. In the non-stormy years 2011 and 2012, anomalies were negative, showing unfavorable conditions for the TC development. Surprisingly, there is an increase in SH anomalies of about 0.45×10^{-3} kg/kg seen in 2015, which creates an inductive condition of TC, but still, no TC was developed at that time. One of the reasons for high SH may be the El Niño conditions, which contributed to more warming

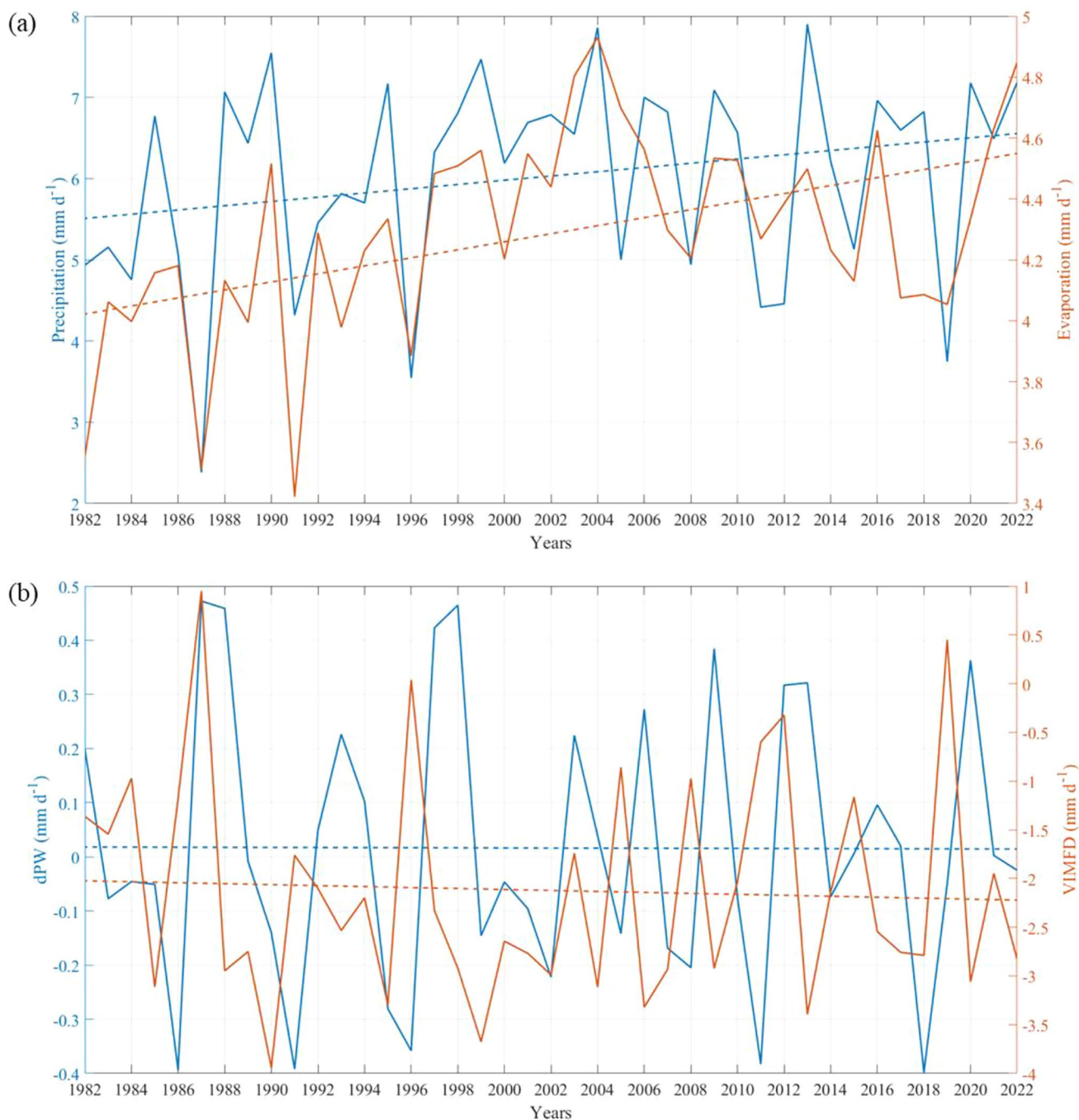


Fig. 2 Time series of (a) Precipitation rate on the left axis and on the right axis Evaporation rate, (b) Precipitable water change (dPW) on the left axis and on the right axis Vertically integrated moisture flux

divergence (VIMFD). The dashed line shows the trend line of the respective parameters

and more evaporation. Figure 6 shows in the case of Fani, 13 days prior, SH at a lower level started increasing; in the case of Amphan, it was 10 days, and in Yaas, it is from 15 days, while in the case of Asani, it was nearly 7 days prior. Similarly, like upper level and lower level for non-stormy years 2011 and 2012, SH anomalies were negative about 1×10^{-3} kg/kg, and for the year 2015, it was higher. An

overall analysis of SH shows that upper-level SH started increasing 6 to 10 before CS development, while for lower level, it is 7 to 13 days before.

MSE is a thermodynamic quantity that combines the effects of both temperature and moisture content in the atmosphere. As moist air rises from the ocean’s surface, it cools and condenses, releasing latent heat. This latent

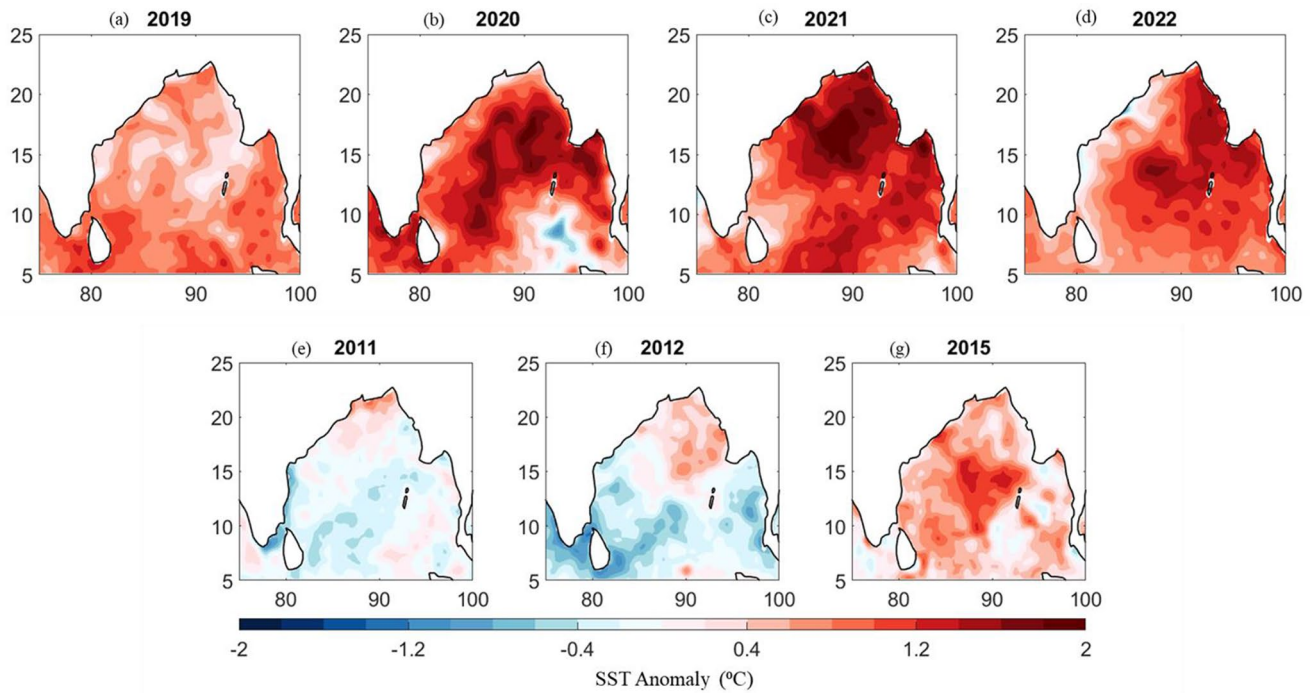


Fig. 3 Time average plot for 15 days prior to CS formation of SST anomalies for the year (a) 2019, (b) 2020, (c) 2021, (d) 2022, (e) 2011, (f) 2012 and (g) 2015

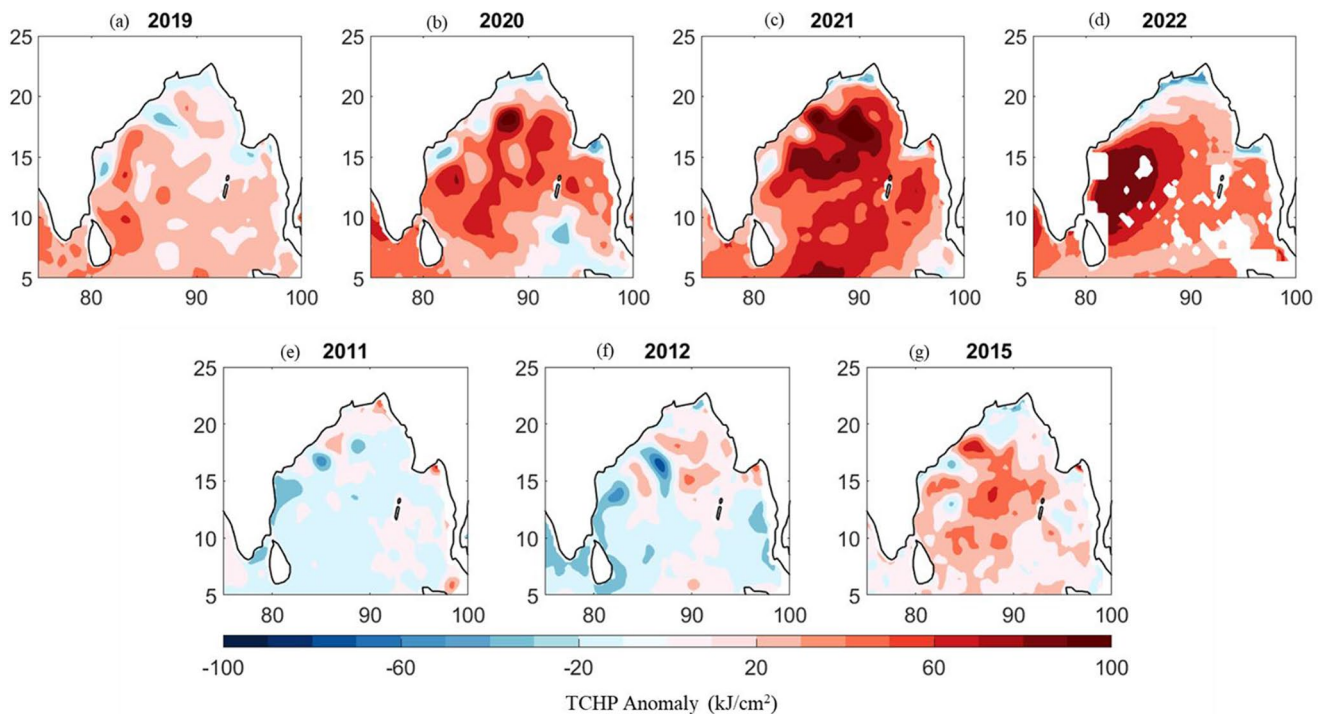


Fig. 4 Same as Fig. 3 but for TCHP anomalies

heat release is a key component of MSE and provides the energy needed to sustain and intensify the storm. As shown in Fig. 7, MSE started increasing nearly 15 days before the development of the CS phase for all the cyclones over the

whole BoB region. Its magnitude increased to 5500 kJ/kg in the case of Amphan and Yaas, and for non-cyclonic years 2011 and 2012, it was negative with the exception of the year 2015, when MSE was high. Upper-level moisture

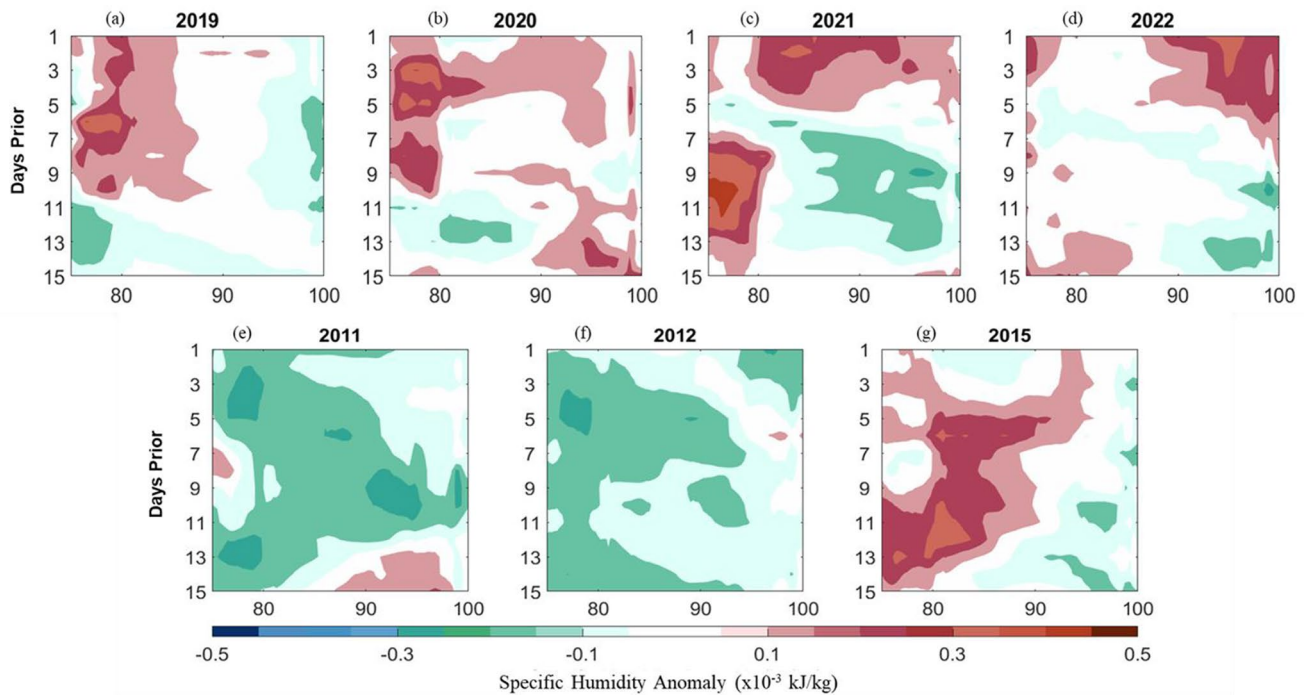


Fig. 5 Hovmöller plot of upper-level specific humidity anomaly for the year (a) 2019, (b) 2020, (c) 2021, (d) 2022, (e) 2011, (f) 2012 and (g) 2015. The plots are averaged on latitudes from 5°N to 25°N. Land regions masked

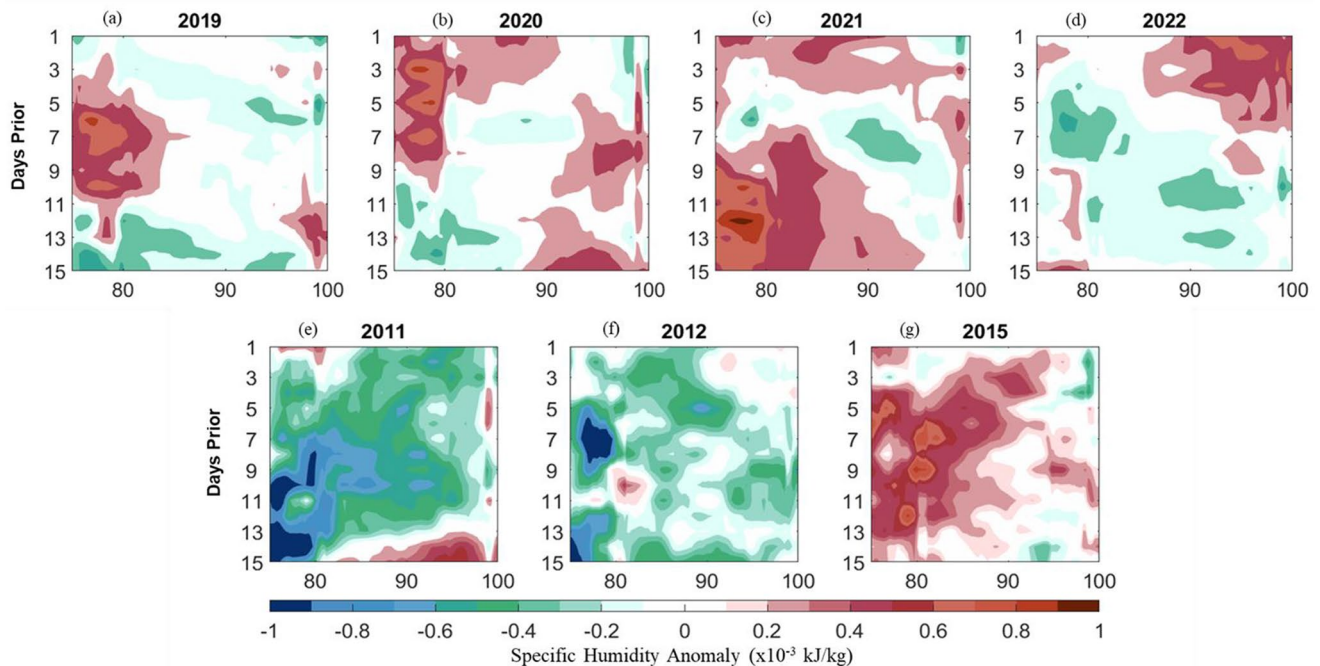


Fig. 6 Same as Fig. 5 but for lower-level specific humidity anomaly

divergence represents the horizontal dispersion or divergence of air masses at elevated altitudes within the Earth's atmosphere. As air parcels diverge horizontally, they ascend and undergo cooling. This cooling process leads to the condensation of water vapour, accompanied by the release

of latent heat energy. This latent heat release serves to intensify the convective activity within cyclonic systems. Importantly, the horizontal divergence of air at upper levels generates a spatial "void". This void acts as a catalyst, drawing air up from lower atmospheric layers to ascend and

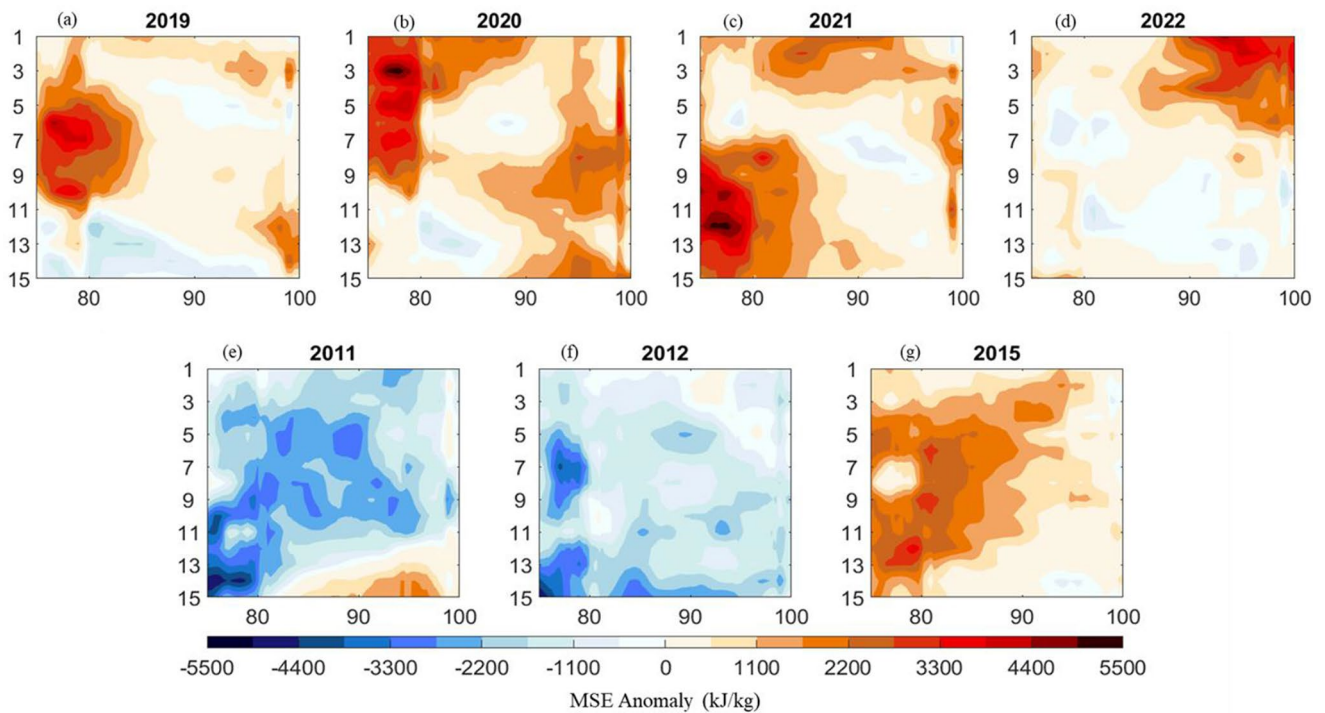


Fig. 7 Same as Fig. 5 but for moist static energy (MSE) anomaly

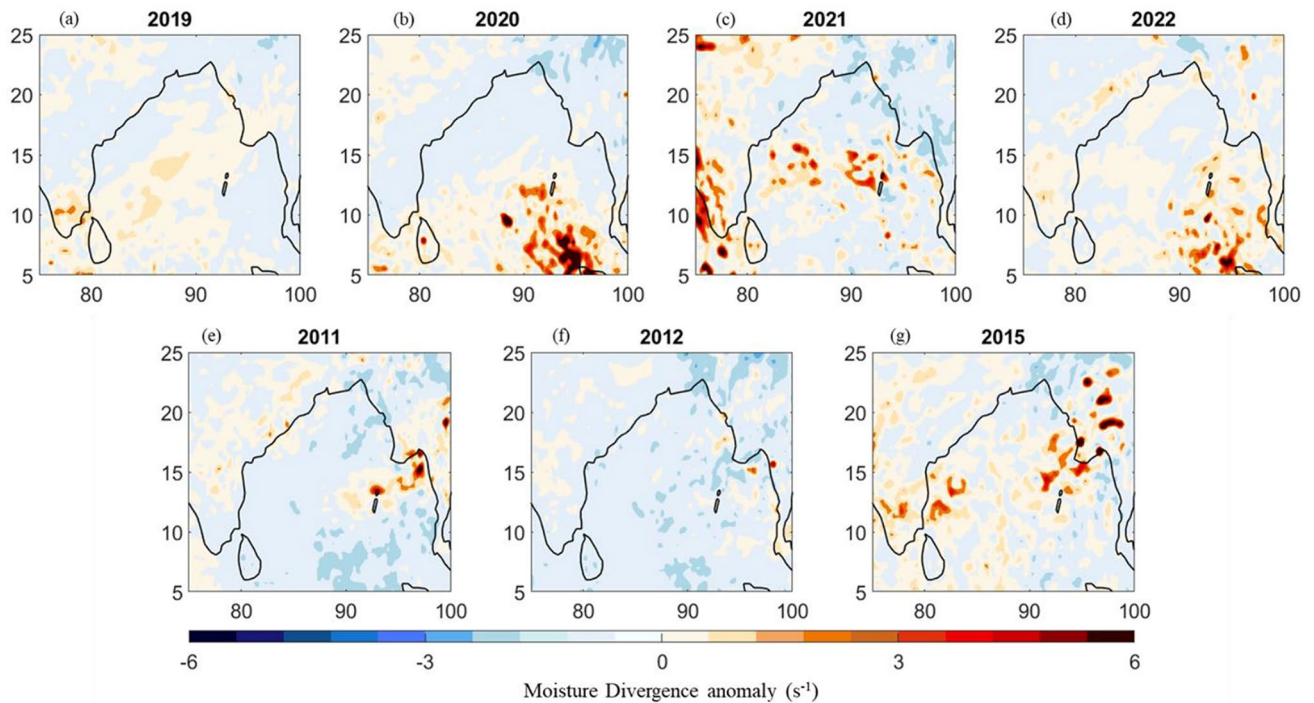


Fig. 8 Same as Fig. 3 but for upper-level moisture divergence anomalies

occupy the void, thereby instigating vertical air movement and the formation of low-pressure systems at the Earth’s surface. While analyzing upper-level moisture divergence anomaly (Fig. 8), it is found that in the case of Fani, it is

been nearly 2 s^{-1} near the central BoB region 15 days prior cyclone, was below 5°N , while in the case of Amphan, a clear and distinct increase of approximately 6 s^{-1} moisture divergence was observed in the southeast sector of BoB.

Yaas showed a moisture divergence of approximately 4 s^{-1} in the central BoB region, while Asani showed a moisture divergence of around 5 s^{-1} in the southeastern BoB. During the years 2011 and 2012, which were characterized by non-stormy conditions, the moisture divergence in the BoB remained consistently negative, ranging from -2 to -2.5 s^{-1} . However, in 2015, there was an exceptional occurrence where the moisture divergence in the BoB was notably high.

Once TC has formed, the positive relative vorticity (RV) helps to keep the storm organized and intense. However, if the relative vorticity decreases, the storm can weaken or dissipate. Figure 9 shows the positive RV anomaly; in the case of Fani (Fig. 9a), RV signatures were not seen. One reason may be that the cyclone was below 5°N , so the signatures were not prominent at that time in BoB. In the case of Amphan (Fig. 9b), positive RV was high ($\sim 40 \times 10^{-6} \text{ s}^{-1}$) near the southeastern region, helping in the intensification of the cyclone. For Yaas (Fig. 9c), positive RV was high ($\sim 12 \times 10^{-6} \text{ s}^{-1}$) near the central BoB, and in the case of Asani (Fig. 9d), it was nearly $16 \times 10^{-6} \text{ s}^{-1}$ in the southeastern region. For the non-stormy cases, no significant signatures of positive RV were observed, which can help in cyclone formation. In 2015, though the other meteorological parameters were very high, the cyclone didn't form, showing that this parameter plays an important role in cyclone formation and intensification but is not sufficient. So, we will further analyze the role of the largest intraseasonal

oscillation, Madden–Julian oscillation (MJO), on cyclone formation and development.

3.3 Madden–Julian Oscillation

The MJO is a large-scale atmospheric disturbance that travels eastward through the tropical oceans every 30–60 days (Madden and Julian 1972, 1994). It is characterized by a cycle of enhanced and suppressed convection (Madden and Julian 1971; Zhou and Chan 2005). The MJO can influence tropical cyclone development by creating a favourable environment for their formation. When the MJO is in an active phase, it increases upward air motion and moisture, necessary for cyclone development (Bhardwaj et al. 2019). The RMM index is a widely used measure of the MJO. An amplitude value greater than 1.0 indicates an active phase of the MJO. For the Indian Ocean, MJO phases 2 and 3 are most favourable for tropical cyclone development.

Figure 10 shows the amplitude and phase characteristics of the MJO within the context of tropical cyclone development in the Bay of Bengal. In the specific instances of Cyclones Fani, Amphan, Yaas, and Asani, we observed intriguing MJO behaviour that influenced their cyclonic intensification. For Cyclone Fani, MJO entered its second phase 12 days prior to the onset of the convective CS phase. Subsequently, it transitioned into the third phase with an amplitude exceeding 1. This amplification of MJO activity significantly contributed to the intensification

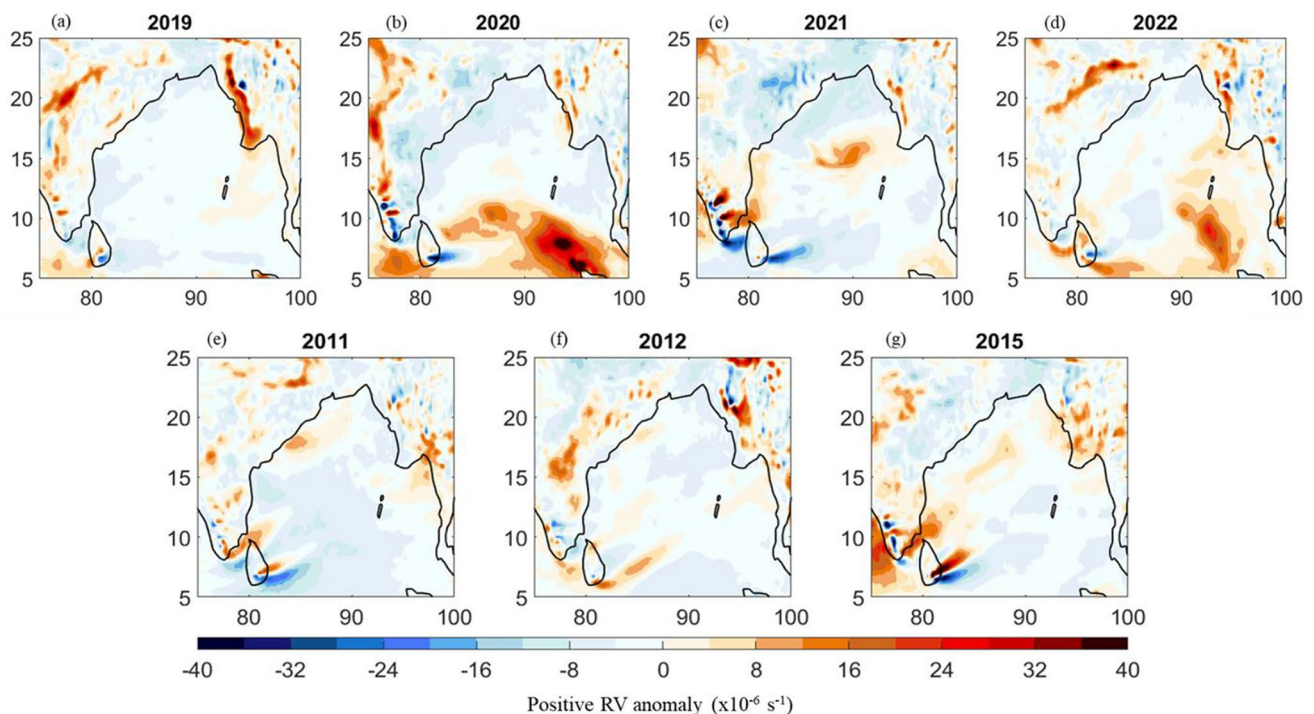


Fig. 9 Same as Fig. 3 but for positive relative vorticity anomalies at 850 hPa

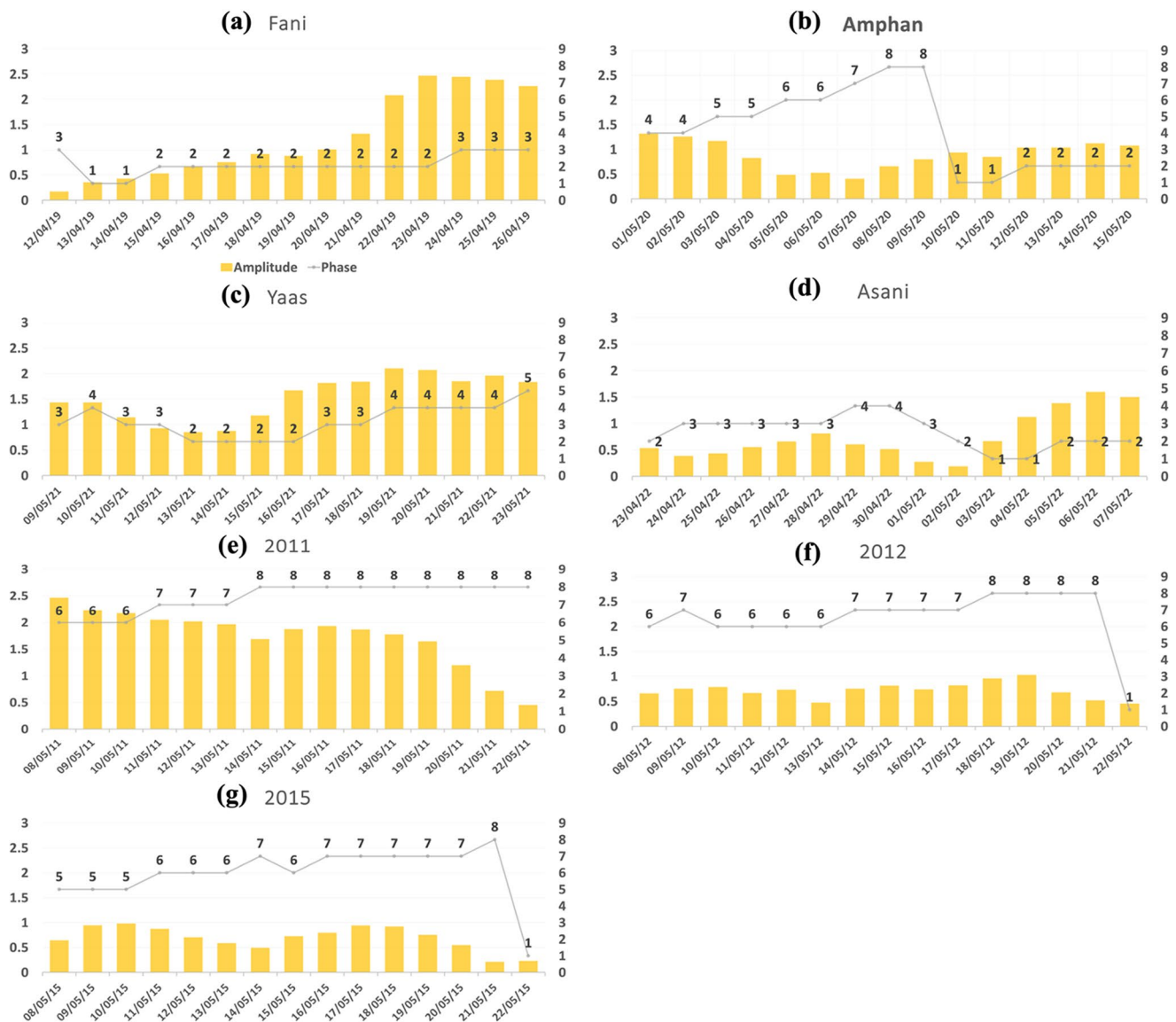


Fig. 10 MJO amplitude (left axis) and phase (right axis) are plotted for (a) Fani, (b) Amphan, (c) Yaas, (d) Asani, (e) 2011, (f) 2012 and (g) 2015

and fortification of Cyclone Fani. In the case of Cyclone Amphan, MJO entered its second phase merely 4 days ahead of the CS phase, accompanied by an amplitude of approximately (1) This relatively subdued MJO presence suggests a less significant role in Cyclone Amphan’s development. Cyclone Yaas experienced MJO entering its third phase a substantial 13 days in advance, followed by transitions into the second and third phases with amplitudes peaking at (2) This sequence of events indicates a pronounced MJO influence on the development of Cyclone Yaas. Cyclone Asani also benefited from MJO dynamics, with MJO entering its second phase with a notable amplitude just 3 days before the CS phase. This timely and vigorous MJO presence aided in the initiation of the cyclonic phase for Cyclone Asani.

In contrast, during non-stormy years, MJO remained predominantly absent from the second or third phases. This absence underscores the significance of MJO during the pre-monsoon season in the context of tropical cyclone development. Notably, in 2015, despite conducive environmental conditions for cyclone formation, cyclonic development was not witnessed due to the lack of MJO activity. This highlights the pivotal role played by the Madden-Julian Oscillation in both the initiation and intensification of tropical cyclones in the Bay of Bengal during the pre-monsoon period. These findings underscore the need for further research and monitoring of MJO patterns to enhance our understanding of cyclone dynamics in this region.

3.4 EOF analysis

The analysis of SST for the month of May, using the EOF method, is presented in Fig. 11a. The results indicate that mode 1 is the most prominent, accounting for a significant 61.8% of the overall variance. The present analysis highlights the increased spatial variability of SST in the BoB, specifically focusing on the central-eastern area. The temporal progression of PC1 shows a prolonged duration of heightened variability that starts from the year 2013. Significantly, current patterns suggest an observable increase in temperature, indicating a widespread and consistent warming occurrence across the Bay of Bengal in recent years. The SST changes observed in this context seem to be influenced by the El Niño-Southern Oscillation (ENSO). The study conducted by Chanda et al. 2018, provides supporting information that establishes a positive association between El Niño phases and sea surface temperature (SST) anomalies.

Figure 11b also matches the spatial pattern of SST variability with mode 1 of 61.4%, showing that the southwestern part of BoB has high variability. The temporal variance

also shows the increased variability in recent decades. The upper-level moisture is increasing, as observed in the trend plot (Fig. 1b), suggesting the variability shows the upper-level moisture increase in the recent decade. Figure 11c shows the first mode accounting for 44.7% of the total variance in wind shear. The analysis reveals a significant disparity between the northern and southern BoB, with negative variance observed in the northern region and positive variance in the southern region. The diminished variance in the northern BoB signifies reduced wind shear, a condition conducive to cyclone intensification. The temporal evolution of PC1 highlights a recent decrease in wind shear, with intermittent positive variance observed in 2021 and 2022.

The IOD is a mode of climatic variability over the Indian Ocean, which is identified by the difference between the Western and Eastern equatorial Indian Oceans in terms of atmospheric pressure and sea surface temperatures. During the positive phase of the IOD, the eastern part of the equatorial Indian Ocean warms, and the western part becomes cooler than usual (PIOD). Conversely, during a negative phase of the IOD (NIOD), the temperature gradient weakens

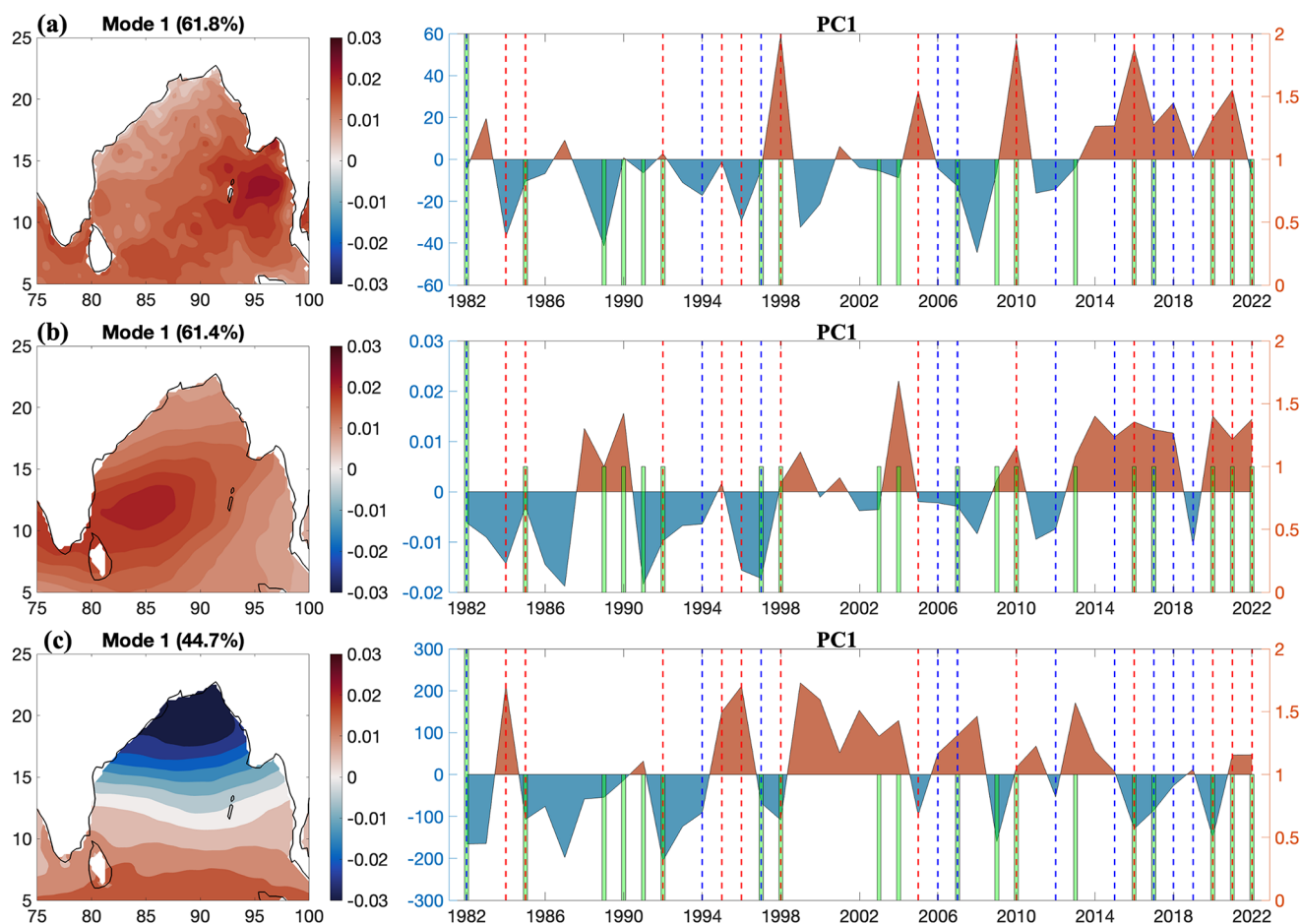


Fig. 11 Spatial EOFs (first mode) and their corresponding PC time series are shown for the (a) SST, (b) upper-level moisture and (c) wind shear. The cyclone frequencies are superimposed on the PC time series,

with the right axis of the PC pane showing cyclone frequency and the left axis showing amplitude. The vertical blue dashed line shows positive IOD years, and the red dashed line shows negative IOD years

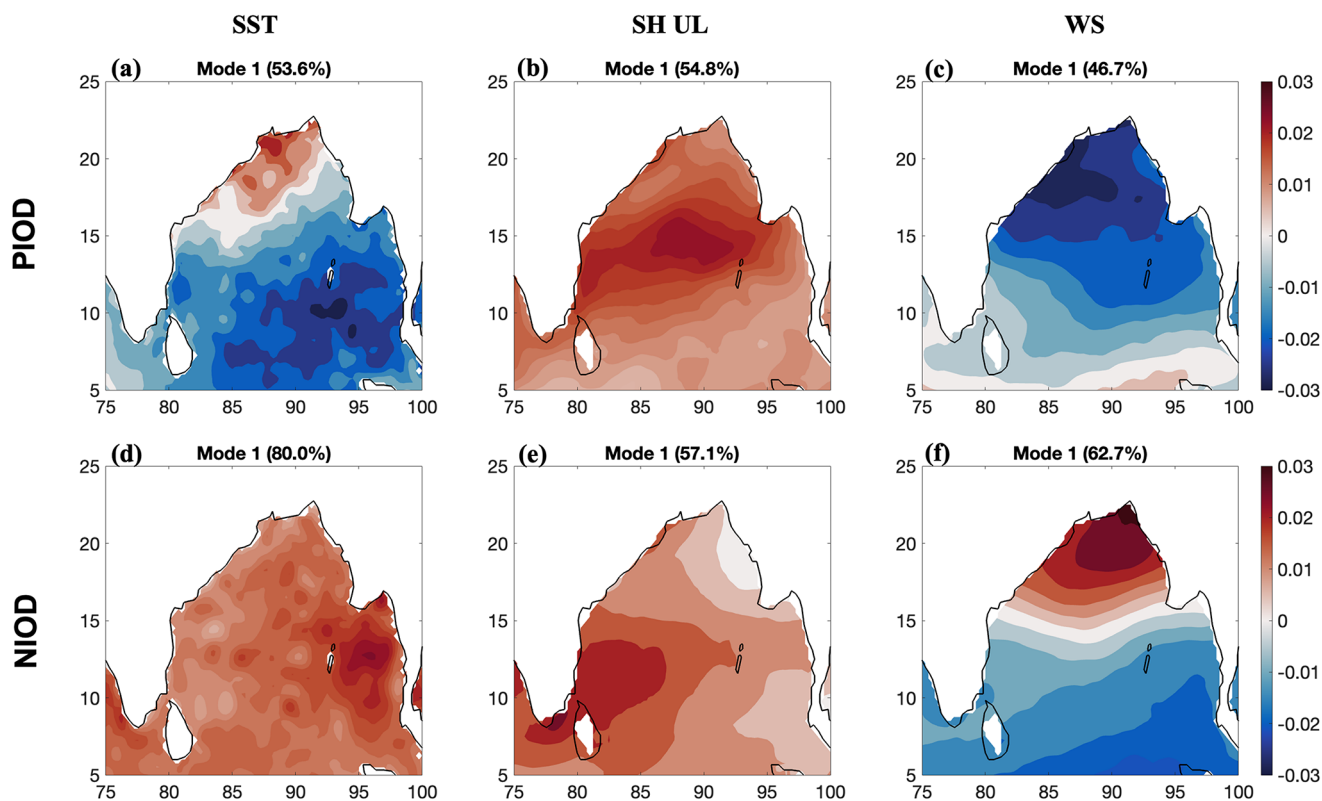


Fig. 12 Spatial EOFs (first mode) are shown for the (a) SST, (b) upper-level moisture, and (c) wind shear for the positive IOD (PIOD) and the same for negative IOD (NIOD) in (d), (e) and (f) respectively

or reverses (Saji et al. 1999). To understand the effect of IOD on the intensification of TCs, EOF analysis is done for PIOD (Fig. 12a, b,c) and NIOD (Fig. 12d, e,f). During PIOD, an inverse variability of 53.6% is observed over central to southern BoB, showing that during PIOD, SST conditions are not that favourable for intensification. Contrary to this, during NIOD, a strong positive SST variability of 80% is observed in favour of cyclone intensification. Upper-level moisture in both cases shows positive variability (Fig. 12b); in the case of NIOD, it is more towards southern BoB but not very distinct (Fig. 12e), which indicates that in general, the IOD phase does not have much significant influence on the upper level of moisture during the pre-monsoon month of May. The wind shear showed a high negative variability of 62.7% for NIOD over central to the southern bay, showing more conducive conditions for TC intensification, whereas, during PIOD, the variability is negative but more towards the northern BoB.

The overall EOF analysis for all 41 years of these meteorological variables and cyclone frequency reveals a consistent and interconnected depiction. In recent years, more favourable conditions for cyclone intensification in the BoB have been witnessed in the month of May. These conditions encompass elevated SST, likely influenced by ENSO, heightened upper-level moisture content, and reduced wind

shear in the northern BoB. More specifically, it has been noted that NIOD has a significant impact on the genesis of highly intensified TCs during IOD events. Recent years have seen a strong relationship between NIOD events and pre-monsoon TC, as well as peak variability of SST and upper-level moisture particularly over BoB (Fig. 11). These findings provide support to the hypothesis that NIOD is one of the important contributors to intensification, although pre-monsoon TC Fani formed in 2019 during a PIOD event. This, however, is a general pattern that necessitates further investigation.

4 Conclusions

A 41-year dataset (1982–2022) examined BoB cyclone formation patterns, uncovering significant trends. SST shows a pronounced, sustained warming trend over four decades. Both upper and lower-level specific humidity rose, while wind shear declined, indicating favourable tropical cyclone conditions. However, recognizing annual fluctuations in these factors remains crucial. The moisture budget shows increased precipitation and evaporation, likely driven by warming scenarios, with slight moisture convergence growth. SST anomalies, vital for cyclone formation, showed

substantial rises in the 15 days preceding events. Fani saw 1–1.2 °C increases, with the most significant warming near the 5°N cyclone formation region. Cyclones Amphan and Yaas experienced even higher SST anomalies, up to 2 °C, while Cyclone Asani peaked at 1.9 °C. Cyclonic years generally featured higher SST anomalies, excluding 2015 due to El Niño conditions. TCHP consistently increased by 70–100 kJ/cm² before cyclone formation, contrasting non-stormy years with negative TCHP values (except 2015). SH anomalies began rising 10–15 days before cyclone formation during cyclonic years, both at upper and lower levels. Non-stormy years typically showed negative SH anomalies, except in 2015, which displayed unusually high SH. MSE increased approximately 15 days pre-cyclone formation across the Bay of Bengal, reaching 5500 kJ/kg for Cyclones Amphan and Yaas. Non-cyclonic years, excluding 2015, featured negative MSE anomalies. Cyclones displayed distinctive moisture divergence patterns in development regions, with non-stormy years consistently negative, except in 2015, which had notably high divergence. Cyclones Amphan, Yaas, and Asani exhibited significant positive RV anomalies in development regions, which non-stormy years did not show.

The MJO played a pivotal role in the BoB cyclone initiation and intensification during the pre-monsoon season. Active MJO phases over the Bay of Bengal favoured cyclogenesis and intensification, as observed in recent cyclones Fani, Amphan, Yaas, and Asani. In contrast, non-stormy years lacked MJO activity in phases 2 and 3, underscoring its importance in cyclone development. Notably, despite favourable conditions, 2015 did not witness cyclone formation due to the absence of MJO activity. EOF analysis for May in the Bay of Bengal indicated increasingly favourable conditions for cyclone intensification in recent years, and during NIOD, SST and wind shear conditions are much more favourable for intensification. However, not much influence on the moisture variability is found in either phase of the IOD. Furthermore, in recent years conducive conditions for TC intensification are distinct during the month of May and are associated with NIOD. The study highlights the Bay of Bengal's evolving climatic patterns influencing cyclone formation. Warming SST, rising specific humidity, reduced wind shear, and increasing moisture convergence create conducive conditions. SST anomalies, TCHP, SH, MSE, and MJO activity play pivotal roles in cyclone development. Understanding these factors is vital for enhancing cyclone prediction and preparedness in the region.

Acknowledgements The authors acknowledge the support from IIT Bhubaneswar, the Ministry of Earth Sciences (MoES) Government of India, and the New Venture Fund to carry out this research work. The authors are also grateful to Copernicus Climate Data Store, the Indian Space Research Organization (ISRO), the Australian Bureau of

Meteorology (BoM), the Japan Meteorological Agency (JMA), and the India Meteorological Department (IMD) for providing the datasets to carry out this study.

Data availability Monthly ocean heat content obtained from Ocean Reanalysis System 5 (ORAS5) (available from <https://cds.climate.copernicus.eu/cdsapp#!/dataset/reanalysis-oras5>). Tropical Cyclone Heat Potential (TCHP) daily data are collected from the Bhuvan portal (available from <https://bhuvan-app3.nrsc.gov.in/data/download/index.php>). Madden Julian Oscillation (MJO) data available from the Australian Bureau of Meteorology (<http://www.bom.gov.au/climate/mjo/>). Optimum interpolation Sea Surface Temperature (SST) data available from <https://psl.noaa.gov/data/gridded/data.noaa.oisst.v2.highres.html>.

References

- Back LE, Bretherton CS (2006) Geographic variability in the export of moist static energy and vertical motion profiles in the tropical Pacific. *Geophys Res Lett* 17. <https://doi.org/10.1029/2006gl026672>
- Balaguru K, Foltz GR, Leung LR, Emanuel KA (2016) Global warming-induced upper-ocean freshening and the intensification of super typhoons. *Nat Commun* 1. <https://doi.org/10.1038/ncomms13670>
- Banacos PC, Schultz DM (2005) The use of moisture flux convergence in forecasting convective initiation: historical and operational perspectives. *Wea Forecast* 3:351–366. <https://doi.org/10.1175/waf858.1>
- Berry G, Reeder MJ (2014) Objective identification of the Inter-tropical Convergence Zone: Climatology and trends from the ERA-Interim. *J Clim* 5:1894–1909. <https://doi.org/10.1175/jcli-d-13-00339.1>
- Bhardwaj P, Singh O, Pattanaik DR, Klotzbach PJ (2019) Modulation of bay of bengal tropical cyclone activity by the madden-julian the oscillation. *Atmos Res* 23–38. <https://doi.org/10.1016/j.atmosres.2019.06.010>
- Chakraborty T, Pattnaik S, Baisya H, Vishwakarma V (2022) Investigation of ocean sub-surface processes in Tropical Cyclone Phailin using a coupled modeling Framework: sensitivity to Ocean conditions. *Oceans* 3:364–388. <https://doi.org/10.3390/oceans3030025>
- Chanda A, Das S, Mukhopadhyay A, Ghosh A, Akhand A, Ghosh P, Ghosh T, Mitra D, Hazra S (2018) Sea surface temperature and rainfall anomaly over the Bay of Bengal during the El Niño-Southern Oscillation and the extreme Indian Ocean Dipole events between 2002 and 2016. *Remote Sens Appl Soc Environ* 10–22. <https://doi.org/10.1016/j.rsase.2018.08.001>
- Chowdhury AMR, Bhuyia AU, Choudhury AY, Sen R (1993) The Bangladesh Cyclone of 1991: why so many people died. *Disasters* 4:291–304. <https://doi.org/10.1111/j.1467-7717.1993.tb00503.x>
- Copernicus Climate Change Service, Climate Data Store (2021) ORAS5 global ocean reanalysis monthly data from 1958 to present. Copernicus Climate Change Service (C3S) Climate Data Store (CDS). <https://doi.org/10.24381/cds.67e8eeb7>. Accessed 22-07-2023
- Fanchiotti M, Dash J, Tompkins EL, Hutton CW (2020) The 1999 super cyclone in Odisha, India: a systematic review of documented losses. *Int J Disaster Risk Reduct* 101790. <https://doi.org/10.1016/j.ijdrr.2020.101790>
- Hersbach H, Bell B, Berrisford P, Biavati G, Horányi A, Muñoz Sabater J, Nicolas J, Peubey C, Radu R, Rozum I, Schepers D, Simmons A, Soci C, Dee D, Thépaut J-N (2023) ERA5 monthly averaged data on pressure levels from 1940 to present. Copernicus Climate

- Change Service (the C3S) Climate Data Store (CDS). <https://doi.org/10.24381/cds.6860a573>. Accessed 22-07-2023
- Hossain N (2017) The 1970 Bhola cyclone, nationalist politics, and the subsistence crisis contract in Bangladesh. *Disasters* 1:187–203. <https://doi.org/10.1111/disa.12235>
- Huang B, Liu C, Banzon V, Freeman E, Graham G, Hankins B, Smith T, Zhang H-M (2021) Improvements of the Daily Optimum Interpolation Sea Surface temperature (DOISST) version 2.1. *J Clim* 8:2923–2939. <https://doi.org/10.1175/jcli-d-20-0166.1>
- Iskandar I, Lestari D, Utari P, Sari Q, Setiabudidaya D, Mardiansyah W, Supardi R (2018) How strong was the 2015/2016 El Niño event? *J Phys Conf Ser* 012030. <https://doi.org/10.1088/1742-6596/1011/1/012030>
- Knutson T, Camargo SJ, Chan JCL, Emanuel K, Ho C-H, Kossin J, Mohapatra M, Satoh M, Sugi M, Walsh K, Wu L (2020) Tropical Cyclones and Climate Change Assessment: part II: projected response to anthropogenic warming. *B Am Meteorol Soc* 3:E303–E322. <https://doi.org/10.1175/bams-d-18-0194.1>
- Lorenz EN (1956) Empirical orthogonal functions and statistical weather prediction, vol 1. Massachusetts Institute of Technology, Department of Meteorology, Cambridge, p 52
- Madden RA, Julian PR (1971) Detection of a 40–50 day oscillation in the Zonal wind in the Tropical Pacific. *J Atmos Sci* 5:702–708. [https://doi.org/10.1175/1520-0469\(1971\)028%3C0702:doadoi%3E2.0.co;2](https://doi.org/10.1175/1520-0469(1971)028%3C0702:doadoi%3E2.0.co;2)
- Madden RA, Julian PR (1972) Description of Global-Scale Circulation Cells in the Tropics with a 40–50 day period. *J Atmos Sci* 6:1109–1123. [https://doi.org/10.1175/1520-0469\(1972\)029%3C1109:dogsc%3E2.0.co;2](https://doi.org/10.1175/1520-0469(1972)029%3C1109:dogsc%3E2.0.co;2)
- Madden RA, Julian PR (1994) Observations of the 40–50-Day Tropical Oscillation—A Review. *Mon Weather Rev* 5:814–837. [https://doi.org/10.1175/1520-0493\(1994\)122%3C0814:ootdo%3E2.0.co;2](https://doi.org/10.1175/1520-0493(1994)122%3C0814:ootdo%3E2.0.co;2)
- Mishra T, Malakar K (2020) Loss and damages from Cyclone: a Case Study from Odisha, a Coastal State. *Dev Coastal Zones Disaster Manage* 281–291. https://doi.org/10.1007/978-981-15-4294-7_19
- Mondal M, Biswas A, Halder S, Mandal S, Bhattacharya S, Paul S (2022) Spatio-temporal behaviours of tropical cyclones over the bay of Bengal Basin in last five decades. *Trop Cyclone Res Rev* 1:1–15. <https://doi.org/10.1016/j.tcr.2021.11.004>
- Neelin JD, Held IM (1987) Modeling tropical convergence based on the Moist Static Energy Budget. *Mon Weather Rev* 1:3–12. [https://doi.org/10.1175/1520-0493\(1987\)115%3C0003:mtcbot%3E2.0.co;2](https://doi.org/10.1175/1520-0493(1987)115%3C0003:mtcbot%3E2.0.co;2)
- Priya P, Pattnaik S, Trivedi D (2022) Characteristics of the tropical cyclones over the North Indian Ocean Basins from the long-term datasets. *Meteor Atmos Phys* 4. <https://doi.org/10.1007/s00703-022-00904-7>
- Rai D, Pattnaik S, Rajesh PV (2016) Sensitivity of tropical cyclone characteristics to the radial distribution of sea surface temperature. *J Earth Syst Sci* 4:691–708. <https://doi.org/10.1007/s12040-016-0687-9>
- Saji NH, Goswami BN, Vinayachandran PN, Yamagata T (1999) A dipole mode in the tropical Indian Ocean. *Nature* 6751:360–363. <https://doi.org/10.1038/43854>
- Vishwakarma V, Pattnaik S (2022) Role of large-scale and microphysical precipitation efficiency on rainfall characteristics of tropical cyclones over the Bay of Bengal. *Nat Hazards* 2:1585–1608. <https://doi.org/10.1007/s11069-022-05439-z>
- Vishwakarma V, Pattnaik S, Chakraborty T, Joseph S, Mitra AK (2022) Impacts of sea-surface temperatures on rapid intensification and mature phases of super cyclone Amphan (2020). *J Earth Syst Sci* 1. <https://doi.org/10.1007/s12040-022-01816-1>
- Wada A, Usui N (2007) Importance of tropical cyclone heat potential for tropical cyclone intensity and intensification in the western North Pacific. *J Oceanogr* 3:427–447. <https://doi.org/10.1007/s10872-007-0039-0>
- Wang Z, Zhao J, Huang H, Wang X (2022) A review on the application of machine learning methods in Tropical Cyclone forecasting. *Front Earth Sci*. <https://doi.org/10.3389/feart.2022.902596>
- Wheeler MC, Hendon HH (2004) An all-season real-time multi-variate MJO Index: development of an index for monitoring and prediction. *Mon Weather Rev* 8:1917–1932. [https://doi.org/10.1175/1520-0493\(2004\)132%3C1917:aarmmi%3E2.0.co;2](https://doi.org/10.1175/1520-0493(2004)132%3C1917:aarmmi%3E2.0.co;2)
- World Meteorological Organization (2008) Tropical cyclone operational plan for the Bay of Bengal and the Arabian Sea. Document No. WMO/TD No. 84, pp TCP–21
- Zhou W, Chan JCL (2005) Intraseasonal oscillations and the South China Sea summer monsoon onset. *Int J Climatol* 12:1585–1609. <https://doi.org/10.1002/joc.1209>

Publisher's note Springer Nature remains neutral with regard to jurisdictional claims in published maps and institutional affiliations.

Springer Nature or its licensor (e.g. a society or other partner) holds exclusive rights to this article under a publishing agreement with the author(s) or other rightsholder(s); author self-archiving of the accepted manuscript version of this article is solely governed by the terms of such publishing agreement and applicable law.